OPEN ACCESS
IOP Publishing
Inverse Problems
Inverse Problems **37** (2021) 115005 (19pp)
https://doi.org/10.1088/1361-6420/ac2d75

A source reconstruction method in two dimensional radiative transport using boundary data measured on an arc

Hiroshi Fujiwara[1], **Kamran Sadiq**[2,*] **and Alexandru Tamasan**[3]

[1] Graduate School of Informatics, Kyoto University, Yoshida Honmachi, Sakyo-ku, Kyoto 606-8501, Japan
[2] Johann Radon Institute of Computational and Applied Mathematics (RICAM), Altenbergerstrasse 69, 4040 Linz, Austria
[3] Department of Mathematics, University of Central Florida, Orlando, 32816 Florida, United States of America

E-mail: fujiwara@acs.i.kyoto-u.ac.jp, kamran.sadiq@ricam.oeaw.ac.at and tamasan@math.ucf.edu

Received 6 September 2021
Accepted for publication 6 October 2021
Published 21 October 2021

Abstract

We consider an inverse source problem in the stationary radiating transport through a two dimensional absorbing and scattering medium. Of specific interest, the exiting radiation is measured on an arc. The attenuation and scattering properties of the medium are assumed known. For scattering kernels of finite Fourier content in the angular variable, we show how to quantitatively recover the part of the isotropic sources restricted to the convex hull of the measurement arc. The approach is based on the Cauchy problem with partial data for a Beltrami-like equation associated with A-analytic maps in the sense of Bukhgeim, and extends authors' previous work to this specific partial data case. The robustness of the method is demonstrated by the results of several numerical experiments.

Keywords: radiative transport, source reconstruction, scattering, A-analytic maps, Hilbert transform, optical molecular imaging, bioluminescence tomography

(Some figures may appear in colour only in the online journal)

*Author to whom any correspondence should be addressed.

Original content from this work may be used under the terms of the Creative Commons Attribution 4.0 licence. Any further distribution of this work must maintain attribution to the author(s) and the title of the work, journal citation and DOI.

1. Introduction

Let Ω be a strictly convex planar domain. In the steady state case, when generated solely by a source f inside Ω, the density $u(z,\boldsymbol{\theta})$ of particles at z traveling in the direction $\boldsymbol{\theta}$ through an absorbing and scattering domain Ω solves the stationary transport boundary value problem

$$\begin{aligned} &\boldsymbol{\theta}\cdot\nabla u(z,\boldsymbol{\theta}) + a(z,\boldsymbol{\theta})u(z,\boldsymbol{\theta}) - \int_{\mathbf{S}^1} k(z,\boldsymbol{\theta},\boldsymbol{\theta}')u(z,\boldsymbol{\theta}')\mathrm{d}\boldsymbol{\theta}' = f(z,\boldsymbol{\theta}), \quad (z,\boldsymbol{\theta})\in\Omega\times\mathbf{S}^1, \\ &u|_{\Gamma_-} = 0, \end{aligned} \tag{1}$$

where $\Gamma_- := \{(\zeta,\boldsymbol{\theta})\in\partial\Omega\times\mathbf{S}^1 : \nu(\zeta)\cdot\boldsymbol{\theta} < 0\}$ with ν being the outer unit normal field at the boundary. The boundary condition indicates that no radiation is coming from outside Ω. Throughout, the measure on the circle is normalized to $\int_{\mathbf{S}^1}\mathrm{d}\boldsymbol{\theta} = 1$.

The boundary value problem (1) is known to have a unique solution under various 'subcritical' assumptions, e.g., [1, 5–7, 9, 21], with a general result in [31] showing that, for an open and dense set of coefficients $a\in C^2(\overline{\Omega}\times\mathbf{S}^1)$ and $k\in C^2(\overline{\Omega}\times\mathbf{S}^1\times\mathbf{S}^1)$, the problem (1) has a unique solution $u\in L^2(\Omega\times\mathbf{S}^1)$ for any $f\in L^2(\Omega\times\mathbf{S}^1)$. Some of our arguments in the reconstruction method here require solutions $u\in C^{1,\mu}(\overline{\Omega}\times\mathbf{S}^1)$, $\frac{1}{2}<\mu<1$. We revisit the arguments in [31] and show that such a regularity can be achieved for sources $f\in W^{2,p}(\Omega\times\mathbf{S}^1)$, $p>4$; see theorem 2.2 (b) below.

For an arc Λ of the boundary of Ω, we consider the inverse problem of determining f from measurements of exiting radiation g on Λ:

$$u|_{\Lambda_+} = g, \tag{2}$$

where $\Lambda_+ := \{(z,\boldsymbol{\theta})\in\Lambda\times\mathbf{S}^1 : \nu(z)\cdot\boldsymbol{\theta} > 0\}$ with ν being the outer unit normal field at the boundary.

When full boundary data is available ($\Lambda = \partial\Omega$) the problem has been well studied, e.g., [2, 12, 19, 31] in Euclidean domains, and [22, 29] in refractive media (Riemannian domains).

In the partial data case, there are only two results: the work in [16] formulates a local tomography question, and establishes unique determination of the wavefront set of the source in a specific subdomain (called visible set). Moreover, if the source is *a priori* known to be supported in this visible set, and the medium has an analytic attenuation coefficient, then the source is uniquely determined by the specific partial data. In contrast, we provide a quantitative reconstruction method where the source may also be supported outside this visible set, and the attenuation is merely twice differentiable. The work in [30] formulates the partial data problem for a slab domain, and reconstructs a source from known data on each side on sufficiently long intervals. In contrast, our method here assumes only 'one sided' boundary data, and does not require iterative solvability of the forward problem.

The problem formulated here is the two dimensional version of the corresponding three dimensional problem occurring in imaging techniques such as bioluminescence tomography and optical molecular imaging, see [15, 17, 35] and references therein.

Except for the results in section 2, which concern the forward problem, in this work the source and attenuation coefficient are assumed isotropic, $f = f(z)$ and $a = a(z)$, and that the scattering kernel $k(z,\boldsymbol{\theta},\boldsymbol{\theta}') = k(z,\boldsymbol{\theta}\cdot\boldsymbol{\theta}')$ depends polynomially on the angle between the directions,

$$k(z,\cos\theta) = k_0(z) + 2\sum_{n=1}^{M} k_{-n}(z)\cos(n\theta), \tag{3}$$

for some fixed integer $M \geqslant 1$. Moreover, the functions a, f, k are assumed real valued. These assumptions occur naturally in radiative transfer models in optics, see, e.g. [4].

Our main result, theorem 4.1, shows that $u|_{\Lambda_+}$ determines both f and u in the convex hull of Λ, and provides a method of reconstruction. Specific to two dimensional domains, our approach is based on the Cauchy problem with partial data for a Beltrami-like equation associated with A-analytic maps in the sense of Bukhgeim [3], and extends the authors' previous work [12], which used measurements on the entire boundary, to this specific partial data case. More precisely, for scattering kernels of finite Fourier content as in (3), we prove that the trace $u|_\Lambda$ determines u on the chord joining the endpoints of Λ. The role of the finite Fourier content has been independently recognized in [22].

As demonstrated by the numerical experiments in section 5, the method is robust with respect to the modeling error, in the sense that it reconstructs discontinuous sources, even when embedded in media with a *discontinuous* absorption property, and with a scattering kernel of *infinite* Fourier content in the angular variable. For the particular choice of coefficients, the method is also robust with respect to an added relative error in the L^2 sense of 5.1%.

2. Remarks on the existence and regularity of the forward problem

In the absence of some subcritical assumption, the well posedness in $L^p(\Omega \times \mathbf{S}^1)$ of the boundary value problem (1) relies on the following compactness result, proven in [31, lemma 2.4] for the case $p = 2$ and a and k twice differentiable. In this section we revisit the arguments in [31] for any $1 < p < \infty$, and show that they hold if the attenuation is merely *once* differentiable. We work in two dimensions but this is not essential. Adopting the notation in [31], let us consider the operators

$$\begin{aligned} [T_1^{-1}\psi](x,\boldsymbol{\theta}) &= \int_{-\infty}^{0} e^{-\int_s^0 a(x+t\boldsymbol{\theta},\boldsymbol{\theta})\mathrm{d}t}\psi(x+s\boldsymbol{\theta},\boldsymbol{\theta})\mathrm{d}s, \quad \text{and} \\ [K\psi](x,\boldsymbol{\theta}) &= \int_{\mathbf{S}^1} k(x,\boldsymbol{\theta},\boldsymbol{\theta}')\psi(x,\boldsymbol{\theta}')\mathrm{d}\boldsymbol{\theta}', \end{aligned} \tag{4}$$

where the intervening functions are extended by 0 outside Ω.

Using the formal expansion

$$u = T_1^{-1}f + T_1^{-1}KT_1^{-1}f + T_1^{-1}(KT_1^{-1}K)[I - T_1^{-1}K]^{-1}T_1^{-1}f, \tag{5}$$

the well posed-ness in $L^p(\Omega \times \mathbf{S}^1)$ of the boundary value problem (1) reduces to the invertibility of $I - T_1^{-1}K$ in $L^p(\Omega \times \mathbf{S}^1)$.

To further simplify notations, let $\widehat{x} = \frac{x}{|x|}$, so that for $y \neq x$ we have $y = x - |x-y|(\widehat{x-y})$.

Proposition 2.1. *Let $a \in C^1(\overline{\Omega} \times \mathbf{S}^1)$ and $k \in C^2(\overline{\Omega} \times \mathbf{S}^1 \times \mathbf{S}^1)$. Then the operator*

$$KT_1^{-1}K : L^p(\Omega \times \mathbf{S}^1) \to W^{1,p}(\Omega \times \mathbf{S}^1) \textit{ is bounded}, \ 1 < p < \infty. \tag{6}$$

Proof. Using the definitions of T_1^{-1} and K above, and a change to polar coordinates, one can write

$$[KT_1^{-1}K\psi](x,\boldsymbol{\theta}) = \int_{\mathbf{S}^1}\int_{\Omega} \frac{\eta\left(x, |x-y|, (\widehat{x-y}), \boldsymbol{\theta}, \boldsymbol{\theta}'\right)}{|x-y|}\psi\left(y, \boldsymbol{\theta}'\right)\mathrm{d}y\,\mathrm{d}\boldsymbol{\theta}', \tag{7}$$

where, for $\left(x, r, \boldsymbol{\alpha}, \boldsymbol{\theta}, \boldsymbol{\theta}'\right) \in \Omega \times [0, \infty) \times \mathbf{S}^1 \times \mathbf{S}^1 \times \mathbf{S}^1$,

$$\eta\left(x, r, \boldsymbol{\alpha}, \boldsymbol{\theta}, \boldsymbol{\theta}'\right) = e^{-\int_0^r a(x-t\boldsymbol{\alpha},\boldsymbol{\alpha})\mathrm{d}t} k\left(x, \boldsymbol{\theta}, \boldsymbol{\alpha}\right) k\left(x - r\boldsymbol{\alpha}, \boldsymbol{\alpha}, \boldsymbol{\theta}'\right).$$

An application of the fundamental theorem of calculus to $r \mapsto \eta\left(x, r, \boldsymbol{\alpha}, \boldsymbol{\theta}, \boldsymbol{\theta}'\right)$ yields

$$\eta\left(x, r, \boldsymbol{\alpha}, \boldsymbol{\theta}, \boldsymbol{\theta}'\right) = \eta\left(x, 0, \boldsymbol{\alpha}, \boldsymbol{\theta}, \boldsymbol{\theta}'\right) - rk(x, \boldsymbol{\theta}, \boldsymbol{\alpha})\eta_1\left(x, r, \boldsymbol{\alpha}, \boldsymbol{\theta}'\right), \tag{8}$$

where, for $\boldsymbol{\alpha} = (\alpha_1, \alpha_2)$, the function $\eta_1(x, r, \boldsymbol{\alpha}, \boldsymbol{\theta}')$ is defined by

$$\int_0^1 e^{-\int_0^{r\rho} a(x-t\boldsymbol{\alpha},\boldsymbol{\alpha})\mathrm{d}t} \left[a(x - r\rho\boldsymbol{\alpha}, \boldsymbol{\alpha})k(x - r\rho\boldsymbol{\alpha}, \boldsymbol{\alpha}, \boldsymbol{\theta}') + \sum_{j=1}^{2} \alpha_j \frac{\partial k}{\partial x_j}(x - r\rho\boldsymbol{\alpha}, \boldsymbol{\alpha}, \boldsymbol{\theta}')\right] \mathrm{d}\rho. \tag{9}$$

Note that in η_1 there are no derivatives taken on a, whereas there are first order derivatives on k.

The split of the kernel in (8) induces the split of the operator $KT_1^{-1}K = A - B$ with

$$[A\psi](x, \boldsymbol{\theta}) = \int_{\mathbf{S}^1}\int_{\Omega} \frac{k\left(x, \boldsymbol{\theta}, \widehat{x-y}\right) k\left(x, \widehat{x-y}, \boldsymbol{\theta}'\right)}{|x-y|} \psi\left(y, \boldsymbol{\theta}'\right) \mathrm{d}y\, \mathrm{d}\boldsymbol{\theta}', \quad \text{and}$$

$$[B\psi](x, \boldsymbol{\theta}) = \int_{\mathbf{S}^1}\int_{\Omega} k\left(x, \boldsymbol{\theta}, \widehat{x-y}\right) \eta_1\left(x, |x-y|, \widehat{x-y}, \boldsymbol{\theta}'\right) \psi\left(y, \boldsymbol{\theta}'\right) \mathrm{d}y\, \mathrm{d}\boldsymbol{\theta}',$$

where η_1 is defined in (9).

Using

$$\nabla \frac{1}{|x-y|} = \frac{\widehat{y-x}}{|x-y|^2}, \quad \frac{\partial}{\partial x_j}\left(\frac{x_l - y_l}{|x-y|}\right) = \frac{1}{|x-y|}\left(\delta_{jl} - \frac{(x_j - y_j)(x_l - y_l)}{|x-y|^2}\right),$$

and the regularity $a \in C^1(\overline{\Omega} \times \mathbf{S}^1)$ and $k \in C^2(\overline{\Omega} \times \mathbf{S}^1 \times \mathbf{S}^1)$, by a straightforward calculation of the derivatives, one can verify that $\frac{\partial}{\partial \theta_j}B$ is an operator with bounded kernel, while $\frac{\partial}{\partial x_j}B$ and $\frac{\partial}{\partial \theta_j}A$ are operators with weakly singular kernel, all of which are bounded on $L^p(\Omega \times \mathbf{S}^1)$, e.g., [20, theorem VIII.3.1]. On the other hand, in addition to the terms with weakly singular kernels, the derivatives $\frac{\partial}{\partial x_j}A$ also yield operators of the Calderón–Zygmund type,

$$[\mathcal{C}v](x, \boldsymbol{\theta}) = \int_{\mathbf{S}^1}\int_{\Omega} \frac{\phi(x, \widehat{x-y}, \boldsymbol{\theta}, \boldsymbol{\theta}')}{|x-y|^2} v(y, \boldsymbol{\theta}')\mathrm{d}y\, \mathrm{d}\boldsymbol{\theta}', \tag{10}$$

where the characteristic ϕ satisfies

$$\sup_{\Omega\times\mathbf{S}^1\times\mathbf{S}^1\times\mathbf{S}^1} |\phi(x, \boldsymbol{\alpha}, \boldsymbol{\theta}, \boldsymbol{\theta}')| < \infty. \tag{11}$$

The following lemma concludes the proof of the proposition 2.1. □

Lemma 2.1. *Let $\mathcal{C}$ be the operator in* (10) *with the characteristic ϕ satisfying* (11)*. Then $\mathcal{C}$ is bounded in $L^p(\Omega \times \mathbf{S}^1)$, $p > 1$.*

Proof. For brevity let us introduce the following notations

$$\phi_\infty(x,\boldsymbol{\alpha}) := \sup_{\boldsymbol{\theta},\boldsymbol{\theta}'\in\mathbf{S}^1} |\phi(x,\boldsymbol{\alpha},\boldsymbol{\theta},\boldsymbol{\theta}')|, \quad \psi(y) := \int_{\mathbf{S}^1} |v(y,\boldsymbol{\theta}')| \mathrm{d}\boldsymbol{\theta}', \tag{12}$$

and note that, via the Hölder inequality, $\|\psi\|_{L^p(\Omega)} \leqslant \|v\|_{L^p(\Omega\times\mathbf{S}^1)}$. Using the Calderon–Zygmund boundedness theorem [20, theorem XI.3.1] (the third inequality below), we estimate

$$\begin{aligned}
\|\mathcal{C}v\|^p_{L^p(\Omega\times\mathbf{S}^1)} &\leqslant \int_\Omega \sup_{\boldsymbol{\theta}\in\mathbf{S}^1} |[\mathcal{C}v](x,\boldsymbol{\theta})|^p \mathrm{d}x \leqslant \int_\Omega \left| \int_{\mathbf{S}^1} \int_\Omega \frac{\phi_\infty(x,\widehat{x-y})}{|x-y|^2} |v(y,\boldsymbol{\theta}')| \mathrm{d}y\, \mathrm{d}\boldsymbol{\theta}' \right|^p \mathrm{d}x \\
&= \int_\Omega \left| \int_\Omega \frac{\phi_\infty(x,\widehat{x-y})}{|x-y|^2} \psi(y) \mathrm{d}y \right|^p \mathrm{d}x \leqslant C\|\psi\|^p_{L^p(\Omega)} \\
&\leqslant C\|v\|^p_{L^p(\Omega\times\mathbf{S}^1)}.
\end{aligned}$$

□

The following simple result is useful.

Lemma 2.2. *Let X be a Banach space and $A : X \to X$ be bounded. Then $I \pm A$ have bounded inverses in X, if and only if $I - A^2$ has a bounded inverse in X.*

In particular, for $\lambda \in \mathbb{C}$, the operator $I - T_1^{-1}(\lambda K)$ is invertible in $L^p(\Omega \times \mathbf{S}^1)$ if $I - (T_1^{-1}(\lambda K))^2$ is invertible in $L^p(\Omega \times \mathbf{S}^1)$. By proposition 2.1, $(T_1^{-1}(\lambda K))^2$ is compact for any $\lambda \in \mathbb{C}$. Since $I - (T_1^{-1}(\lambda K))^2$ is invertible for λ in a neighborhood of 0, an application of the analytic Fredholm alternative in Banach spaces, e.g., [8, theorem VII.4.5], yields the following result.

Theorem 2.1. *Let $p > 1$, $a \in C^1(\overline{\Omega} \times \mathbf{S}^1)$, and $k \in C^2(\overline{\Omega} \times \mathbf{S}^1 \times \mathbf{S}^1)$. At least one of the following statements is true.*

(*a*) *$I - T_1^{-1}K$ is invertible in $L^p(\Omega \times \boldsymbol{S}^1)$.*
(*b*) *There exists $\epsilon > 0$ such that $I - T_1^{-1}(\lambda K)$ is invertible in $L^p(\Omega \times \boldsymbol{S}^1)$, for any $0 < |\lambda - 1| < \epsilon$.*

If $a \in C^2(\overline{\Omega} \times \mathbf{S}^1)$, then the regularity of the solution u of (1) increases with the regularity of f as follows.

Theorem 2.2. *Consider the boundary value problem (1) with $a \in C^2(\overline{\Omega} \times \mathbf{S}^1)$. For $p > 1$, let $k \in C^2(\overline{\Omega} \times \mathbf{S}^1 \times \mathbf{S}^1)$ be such that $I - T_1^{-1}K$ is invertible in $L^p(\Omega \times \mathbf{S}^1)$, and let $u \in L^p(\Omega \times \mathbf{S}^1)$ in (5) be the solution of (1).*

(*a*) *If $f \in W^{1,p}(\Omega \times \boldsymbol{S}^1)$, then $u \in W^{1,p}(\Omega \times \boldsymbol{S}^1)$.*
(*b*) *If $f \in W^{2,p}(\Omega \times \boldsymbol{S}^1)$, then $u \in W^{2,p}(\Omega \times \boldsymbol{S}^1)$.*

Proof.

(a) Recall the representation (5) of the solution of (1),

$$u = T_1^{-1}f + T_1^{-1}KT_1^{-1}f + T_1^{-1}[KT_1^{-1}K](I - T_1^{-1}K)^{-1}T_1^{-1}f.$$

It is easy to see that T_1^{-1} and K preserve the space $W^{1,p}(\Omega \times \mathbf{S}^1)$, so that the first two terms belong to $W^{1,p}(\Omega \times \mathbf{S}^1)$. Now, by proposition 2.1, the third term is also in $W^{1,p}(\Omega \times \mathbf{S}^1)$. Note that we only need $a \in C^1(\overline{\Omega} \times \mathbf{S}^1)$ for part (a).

(b) For brevity we introduce the operators

$$T_0^{-1}u(x,\boldsymbol{\theta}) = \int_{-\infty}^{0} u(x+t\boldsymbol{\theta},\boldsymbol{\theta})\mathrm{d}t, \quad K_j u(x,\boldsymbol{\theta}) = \int_{\mathbf{S}^1} \frac{\partial k}{\partial x_j}(x,\boldsymbol{\theta},\boldsymbol{\theta}')u(x,\boldsymbol{\theta}')\mathrm{d}\boldsymbol{\theta}',$$
$$\tilde{T}_0^{-1}u(x,\boldsymbol{\theta}) = \int_{-\infty}^{0} u(x+t\boldsymbol{\theta},\boldsymbol{\theta})t\,\mathrm{d}t, \quad \widehat{K}_j u(x,\boldsymbol{\theta}) = \int_{\mathbf{S}^1} \frac{\partial k}{\partial \theta_j}(x,\boldsymbol{\theta},\boldsymbol{\theta}')u(x,\boldsymbol{\theta}')\mathrm{d}\boldsymbol{\theta}', \quad j=1,2. \tag{13}$$

It is easy to see that $T_0^{-1}, \tilde{T}_0^{-1}, K_j$ and $\widehat{K}_j$ preserve $W^{1,p}(\Omega \times \mathbf{S}^1)$.

By evaluating (1) at $x + t\boldsymbol{\theta}$ and integrating in t from $-\infty$ to 0, the problem (1) with zero incoming fluxes is equivalent to the integral equation.

$$u + T_0^{-1}(au) - T_0^{-1}Ku = T_0^{-1}f. \tag{14}$$

For $f \in W^{1,p}(\Omega \times \mathbf{S}^1)$, according to part (a), $u_{x_j} \in L^p(\Omega \times \mathbf{S}^1)$. In particular u_{x_j} solves the integral equation

$$u_{x_j} + T_0^{-1}(au_{x_j}) - T_0^{-1}Ku_{x_j} = T_0^{-1}f_{x_j} - T_0^{-1}(a_{x_j}u) + T_0^{-1}K_j u. \tag{15}$$

Moreover, since $a \in C^2(\overline{\Omega} \times \mathbf{S}^1)$, $k \in C^2(\overline{\Omega} \times \mathbf{S}^1 \times \mathbf{S}^1)$, and $f \in W^{2,p}(\Omega \times \mathbf{S}^1)$, the right-hand side of (15) lies in $W^{1,p}(\Omega \times \mathbf{S}^1)$. By applying part (a) above, we get that the unique solution to (15)

$$u_{x_j} \in W^{1,p}(\Omega \times \mathbf{S}^1), \quad j=1,2. \tag{16}$$

For $f \in W^{1,p}(\Omega \times \mathbf{S}^1)$, also according to part (a), $u_{\theta_j} \in L^p(\Omega \times \mathbf{S}^1)$. In particular u_{θ_j} is the unique solution of the integral equation

$$u_{\theta_j} + T_0^{-1}(au_{\theta_j}) = T_0^{-1}f_{\theta_j} - \tilde{T}_0^{-1}(au_{x_j}) - \tilde{T}_0^{-1}(a_{x_j}u) - T_0^{-1}(a_{\theta_j}u) + \tilde{T}_0^{-1}K_j u + T_0^{-1}\widehat{K}_j u, \tag{17}$$

which is of the type (14) with $K = 0$. Moreover, since $f \in W^{2,p}(\Omega \times \mathbf{S}^1)$, and, according to (16), $u_{x_j} \in W^{1,p}(\Omega \times \mathbf{S}^1)$, $j = 1,2$, the right-hand side of (17) lies in $W^{1,p}(\Omega \times \mathbf{S}^1)$. Again, by applying part (a), we get

$$u_{\theta_j} \in W^{1,p}(\Omega \times \mathbf{S}^1), \quad j=1,2.$$

Thus, $u \in W^{2,p}(\Omega \times \mathbf{S}^1)$. □

3. Preliminaries

In this section we recall the existing results and concepts used in our reconstruction method.

For $0 < \mu < 1$, and Γ (some part of) the boundary $\partial\Omega$ we consider the Banach spaces:

$$l_\infty^{1,1}(\Gamma) := \left\{ \mathbf{v} = \langle v_0, v_{-1}, v_{-2}, \ldots \rangle \ : \|\mathbf{v}\|_{l_\infty^{1,1}(\Gamma)} := \sup_{\xi\in\Gamma} \sum_{j=0}^{\infty} \langle j \rangle |v_{-j}(\xi)| < \infty \right\},$$

$$C^\mu(\Gamma; l_1) := \left\{ \mathbf{v} = \langle v_0, v_{-1}, v_{-2}, \ldots \rangle : \sup_{\xi\in\Gamma} \|\mathbf{v}(\xi)\|_{l_1} + \sup_{\substack{\xi,\eta\in\Gamma \\ \xi\neq\eta}} \frac{\|\mathbf{v}(\xi) - \mathbf{v}(\eta)\|_{l_1}}{|\xi - \eta|^\mu} < \infty \right\},$$

where, for brevity, we use the notation $\langle j \rangle = (1 + |j|^2)^{1/2}$. We similarly consider $l_\infty^{1,1}(\overline{\Omega})$, $C^\mu(\overline{\Omega}; l_1)$, and $C^\mu(\overline{\Omega}; l_\infty)$.

A sequence valued map $\Omega \ni z \mapsto \mathbf{v}(z) := \langle v_0(z), v_{-1}(z), v_{-2}(z), \ldots \rangle$ in $C(\overline{\Omega}; l_\infty) \cap C^1(\Omega; l_\infty)$ is called $\mathcal{L}^2$-*analytic* (in the sense of Bukhgeim), if

$$\overline{\partial}\mathbf{v}(z) + \mathcal{L}^2 \partial\mathbf{v}(z) = 0, \quad z \in \Omega, \tag{18}$$

where $\mathcal{L}$ is the left shift operator, $\mathcal{L}\langle v_0, v_{-1}, v_{-2}, \ldots \rangle = \langle v_{-1}, v_{-2}, \ldots \rangle$, and $\mathcal{L}^2 = \mathcal{L} \circ \mathcal{L}$. Note that we use the sequences of non-positive indexes to conform with the original notation in Bukhgeim's work [3].

Analogous to the analytic maps, the $\mathcal{L}^2$-analytic maps are determined by their boundary values via a Cauchy-like integral formula [3]. Following [10], the Bukhgeim–Cauchy operator $\mathcal{B}$ acting on $\mathbf{v} = \langle v_0, v_{-1}, v_{-2}, \ldots \rangle$ is defined component-wise for $n \leqslant 0$ by

$$(\mathcal{B}\mathbf{v})_n(z) := \frac{1}{2\pi \mathrm{i}} \int_{\partial\Omega} \frac{v_n(\zeta)}{\zeta - z} \mathrm{d}\zeta + \frac{1}{2\pi \mathrm{i}} \int_{\partial\Omega} \left\{ \frac{\mathrm{d}\zeta}{\zeta - z} - \frac{\mathrm{d}\overline{\zeta}}{\overline{\zeta} - \overline{z}} \right\} \sum_{j=1}^{\infty} v_{n-2j}(\zeta) \left(\frac{\overline{\zeta} - \overline{z}}{\zeta - z} \right)^j, \ z \in \Omega. \tag{19}$$

As shown in [27, theorem 2.2], if $\mathbf{v} = \langle v_0, v_{-1}, v_{-2}, \ldots \rangle \in l_\infty^{1,1}(\partial\Omega) \cap C^\mu(\partial\Omega; l_1)$, then $\mathcal{B}\mathbf{v} \in C^{1,\mu}(\Omega; l_\infty) \cap C(\overline{\Omega}; l_\infty)$ is $\mathcal{L}^2$-analytic in Ω. If $\mathbf{v} \in C^{1,\mu}(\Omega; l_\infty) \cap C(\overline{\Omega}; l_\infty)$ is $\mathcal{L}^2$-analytic in $\overline{\Omega}$, then $\mathbf{v}(z) = \mathcal{B}\mathbf{v}(z)$, for $z \in \overline{\Omega}$.

Also similar to the analytic maps, the traces on the boundary of $\mathcal{L}^2$-analytic maps satisfy some constraints, which can be expressed in terms of a corresponding Hilbert transform introduced in [26]. More precisely, the Bukhgeim–Hilbert transform $\mathcal{H}$ is defined component-wise for $n \leqslant 0$ by

$$(\mathcal{H}\mathbf{v})_n(\xi) = \frac{1}{\pi} \int_{\partial\Omega} \frac{v_n(\zeta)}{\zeta - \xi} \mathrm{d}\zeta + \frac{1}{\pi} \int_{\partial\Omega} \left\{ \frac{\mathrm{d}\zeta}{\zeta - \xi} - \frac{\mathrm{d}\overline{\zeta}}{\overline{\zeta} - \overline{\xi}} \right\} \sum_{j=1}^{\infty} v_{n-2j}(\zeta) \left(\frac{\overline{\zeta} - \overline{\xi}}{\zeta - \xi} \right)^j, \quad \xi \in \Gamma, \tag{20}$$

and we refer to [26] for its mapping properties. For the proof of the theorem below we refer to [26, theorem 3.2].

Theorem 3.1. *Let* $\mathbf{v} = \langle v_0, v_{-1}, v_{-2}, \ldots \rangle \in l_\infty^{1,1}(\partial\Omega) \cap C^\mu(\partial\Omega; l_1)$ *be defined on the boundary* $\partial\Omega$. *Then* $\mathbf{v}$ *is the boundary value of an* $\mathcal{L}^2$-*analytic function if and only if*

$$(I + \mathrm{i}\mathcal{H})\mathbf{v} = \mathbf{0}. \tag{21}$$

In addition to $\mathcal{L}^2$-analytic maps, another ingredient consists in the one-to-one relation between solutions $\mathbf{u} := \langle u_0, u_{-1}, u_{-2}, \ldots \rangle$ to

$$\overline{\partial} u_{-n}(z) + \partial u_{-n-2}(z) + a(z) u_{-n-1}(z) = 0, \quad z \in \Omega,\ n \geqslant 0. \tag{22}$$

and the $\mathcal{L}^2$-analytic map $\mathbf{v}$ satisfying

$$\overline{\partial} v_{-n}(z) + \partial v_{-n-2}(z) = 0, \quad z \in \Omega,\ n \geqslant 0; \tag{23}$$

see [28, lemma 4.2] for details. The relation can be expressed via the convolutions

$$\begin{aligned} v_{-n}(z) &= \sum_{j=0}^{\infty} \alpha_j(z) u_{-n-j}(z), \quad z \in \Omega,\ n \geqslant 0, \\ u_{-n}(z) &= \sum_{j=0}^{\infty} \beta_j(z) v_{-n-j}(z), \quad z \in \Omega,\ n \geqslant 0, \end{aligned} \tag{24}$$

where α_j's and β_j's are the Fourier modes of $e^{\mp h}$,

$$e^{-h(z,\boldsymbol{\theta})} := \sum_{m=0}^{\infty} \alpha_m(z) \mathrm{e}^{\mathrm{i}m\theta}, \quad e^{h(z,\boldsymbol{\theta})} := \sum_{m=0}^{\infty} \beta_m(z) \mathrm{e}^{\mathrm{i}m\theta}, \quad (z,\theta) \in \overline{\Omega} \times \mathbf{S}^1, \tag{25}$$

with h defined by

$$h(z,\boldsymbol{\theta}) := Da(z,\boldsymbol{\theta}) - \frac{1}{2}(I - \mathrm{i}H)\, Ra(z \cdot \boldsymbol{\theta}^{\perp}, \boldsymbol{\theta}^{\perp}). \tag{26}$$

In the above formula, $\boldsymbol{\theta}^{\perp}$ is orthogonal to $\boldsymbol{\theta}$, $Da(z,\boldsymbol{\theta}) = \int_0^{\infty} a(z + t\boldsymbol{\theta})\mathrm{d}t$ is the divergent beam transform of the attenuation a, $Ra(s,\boldsymbol{\theta}^{\perp}) = \int_{-\infty}^{\infty} a\left(s\boldsymbol{\theta}^{\perp} + t\boldsymbol{\theta}\right)\mathrm{d}t$ is the Radon transform of the attenuation a, and H is the (infinite) Hilbert transform

$$Hf(x) = \frac{1}{\pi} \int_{-\infty}^{\infty} \frac{f(s)}{x - s} \mathrm{d}s \tag{27}$$

taken in the first variable and evaluated at $s = z \cdot \boldsymbol{\theta}^{\perp}$. The function h appeared first in [24] and enjoys the crucial property of having vanishing negative Fourier modes. We refer to [28, lemma 4.1] for the properties of h used in here.

The method of reconstruction below considers the operator $[I - \mathrm{i}H_{\mathrm{t}}]$, where H_{t} is the finite Hilbert transform

$$H_{\mathrm{t}} f(x) = \frac{1}{\pi} \int_{-l}^{l} \frac{f(s)}{x - s} \mathrm{d}s, \quad x \in (-l, l), \tag{28}$$

with the integral understood in the sense of principal value. It is well-known ([32]) that $\mathrm{i}H_{\mathrm{t}}$ is a bounded operator on $L^2(-l,l)$ with spectrum $[-1,1]$, see [18, 25]. However, 1 is not in the point spectrum. More precisely,

Proposition 3.1. *On* $L^2(-l,l)$, $\mathrm{Ker}[I - \mathrm{i}H_{\mathrm{t}}] = \{0\}$.

For a proof based on a Riemann–Hilbert problem see [34], or, for an elementary argument see [14].

4. Reconstruction in Ω^+ of a sufficiently smooth isotropic source f

Recall the boundary value problem (1):

$$\begin{aligned} &\boldsymbol{\theta}\cdot\nabla u(z,\boldsymbol{\theta}) + a(z)u(z,\boldsymbol{\theta}) - \int_{\mathbf{S}^1} k(z,\boldsymbol{\theta}\cdot\boldsymbol{\theta}')u(z,\boldsymbol{\theta}')\mathrm{d}\boldsymbol{\theta}' = f(z), \quad (z,\boldsymbol{\theta})\in\Omega\times\mathbf{S}^1,\\ &u|_{\Gamma_-} = 0, \end{aligned} \tag{29}$$

for an isotropic source f and attenuation coefficient a, and with a scattering kernel k of the type (3),

$$k(z,\cos\,\theta) = k_0(z) + 2\sum_{n=1}^{M} k_{-n}(z)\cos(n\theta), \tag{30}$$

for some fixed integer $M \geqslant 1$.

We assume that $a, k_0, k_{-1}, \ldots, k_{-M} \in C^2(\overline{\Omega})$ are such that the forward problem (29) has a unique solution $u \in L^p(\Omega\times\mathbf{S}^1)$ for any $f \in L^p(\Omega)$, see theorem 2.1. We also assume an *unknown* source of *a priori* regularity $f \in W^{2,p}(\Omega)$, $p > 4$. According to theorem 2.2 part (b), $u \in C^{1,\mu}(\Omega\times\mathbf{S}^1)$ with $\mu > 1/2$. In agreement with the physics model, the functions a, f, k are further assumed real valued, so that the solution u is also real valued. Note that, since $k(z,\cos\theta)$ in (30) is both real valued and even in θ, the coefficient k_{-n} in (30) is the $(-n)$th Fourier coefficient of $k(z,\cos(\cdot))$. Moreover k_{-n} is real valued, and $k_n(z) = k_{-n}(z) = \frac{1}{2\pi}\int_{-\pi}^{\pi} k(z,\cos\,\theta)\mathrm{e}^{\mathrm{i}n\theta}\,\mathrm{d}\theta$.

Let $u(z,\boldsymbol{\theta}) = \sum_{-\infty}^{\infty} u_n(z)\mathrm{e}^{\mathrm{i}n\theta}$ be the formal Fourier series representation of the solution of (29) in the angular variable $\boldsymbol{\theta} = (\cos\theta,\ \sin\theta)$. Since u is real valued, $u_{-n} = \overline{u_n}$ and the angular dependence is completely determined by the sequence of its nonpositive Fourier modes

$$\Omega \ni z \mapsto \mathbf{u}(z) := \langle u_0(z), u_{-1}(z), u_{-2}(z), \ldots\rangle. \tag{31}$$

Consider the decomposition of the advection operator $\boldsymbol{\theta}\cdot\nabla = \mathrm{e}^{-\mathrm{i}\theta}\overline{\partial} + \mathrm{e}^{\mathrm{i}\theta}\partial$, where $\overline{\partial} = (\partial_x + \mathrm{i}\partial_y)/2$ and $\partial = (\partial_x - \mathrm{i}\partial_y)/2$ are derivatives in the spatial domain. By identifying the Fourier coefficients of the same order, the equation (29) reduces to the system:

$$\overline{\partial}u_1(z) + \partial u_{-1}(z) + a(z)u_0(z) = k_0(z)u_0(z) + f(z), \tag{32}$$

$$\overline{\partial}u_{-n}(z) + \partial u_{-n-2}(z) + a(z)u_{-n-1}(z) = k_{-n-1}(z)u_{-n-1}(z), \quad 0 \leqslant n \leqslant M-1, \tag{33}$$

$$\overline{\partial}u_{-n}(z) + \partial u_{-n-2}(z) + a(z)u_{-n-1}(z) = 0, \qquad n \geqslant M. \tag{34}$$

Without loss of generality we consider Cartesian coordinates such that Λ lies in the upper half plane with endpoints on the real axis, and let $L = (-l, l)$ be the segment joining the endpoints of the arc. Let $\Omega^+ = \{z \in \Omega:\ \mathbb{I}mz > 0\}$ denote the convex hull of Λ, and note that $\partial\Omega^+ = \Lambda \cup L$.

To simplify the statement of the next result, for each $n \geqslant 0$, let us introduce the functions $F_{-n}(z)$ defined for $z \neq \pm l$ in $\Lambda \cup L$ by

$$F_{-n}(z) := \frac{1}{\mathrm{i}\pi}\int_\Lambda \frac{u_{-n}(\zeta)}{\zeta - z}\mathrm{d}\zeta + \frac{1}{\mathrm{i}\pi}\int_\Lambda \left\{\frac{\mathrm{d}\zeta}{\zeta - z} - \frac{\mathrm{d}\overline{\zeta}}{\overline{\zeta} - \overline{z}}\right\}\sum_{j=1}^{\infty} u_{-n-2j}(\zeta)\left(\frac{\overline{\zeta} - \overline{z}}{\zeta - z}\right)^j. \tag{35}$$

For $z \in \Lambda$, the first integral is in the sense of principal value. Note that F_{-n} is directly determined by the data $u_{-n}|_\Lambda$, $n \geqslant 0$.

The proof of the following result is constructive and provides the basis of the reconstruction method implemented in section 5.

Theorem 4.1. *Let $\Omega \subset \mathbb{R}^2$ be a strictly convex bounded domain, Λ be an arc of its boundary, and Ω^+ be the convex hull of Λ. Consider the boundary value problem (29) for some known real valued $a, k_0, k_{-1}, \ldots, k_{-M} \in C^2(\overline{\Omega})$ such that (29) is well-posed. If the unknown source f is real valued and $W^{2,p}(\Omega)$-regular, with $p > 4$, then $u|_{\Lambda_+}$ uniquely determines f in Ω^+.*

Proof. Let u be the solution of the boundary value problem (29) and $\mathbf{u} = \langle u_0, u_{-1}, u_{-2}, \ldots \rangle$ be the sequence valued map of its non-positive Fourier modes. Since $f \in W^{2,p}(\Omega)$, $p > 4$, then by theorem 2.2 (b), $u \in W^{2,p}(\Omega \times \mathbf{S}^1)$. By the Sobolev embedding, $u \in C^{1,\mu}(\overline{\Omega} \times \mathbf{S}^1)$ with $\mu = 1 - \frac{2}{p} > \frac{1}{2}$, and thus, by [26, proposition 4.1 (i)], $\mathbf{u} \in l^{1,1}_\infty(\partial\Omega^+) \cap C^\mu(\partial\Omega^+; l_1)$.

We note next that the shifted sequence valued map $\mathcal{L}^M\mathbf{u}$ solves

$$\overline{\partial}\mathcal{L}^M\mathbf{u}(z) + \mathcal{L}^2\partial\mathcal{L}^M\mathbf{u}(z) + a(z)\mathcal{L}^{M+1}\mathbf{u}(z) = \mathbf{0}, \quad z \in \Omega, \tag{36}$$

and then the associated sequence valued map $\mathcal{L}^M\mathbf{v} = (v_{-M}, v_{-M-1}, v_{-M-2} \ldots)$ defined by the convolutions (24) solves

$$\overline{\partial}v_{-n}(z) + \partial v_{-n-2}(z) = 0, \quad z \in \Omega,\ n \geqslant M. \tag{37}$$

In particular, $\mathcal{L}^M\mathbf{v}$ is $\mathcal{L}^2$-analytic.

By (2), the data $u|_{\Lambda_+} = g$ on Λ_+ determines $\mathcal{L}^M\mathbf{u}$ on Λ. By the convolution formula (24) for $n \geqslant M$, $\mathcal{L}^M\mathbf{u}|_\Lambda$ determines the traces $\mathcal{L}^M\mathbf{v} \in l^{1,1}_\infty(\Lambda) \cap C^\mu(\Lambda; l_1)$ on Λ.

Since $\mathcal{L}^M\mathbf{v} \in l^{1,1}_\infty(\partial\Omega^+) \cap C^\mu(\partial\Omega^+; l_1)$ is the boundary value of an $\mathcal{L}^2$-analytic function in Ω^+, then the necessity part of theorem 3.1 yields

$$[I + \mathrm{i}\mathcal{H}]\mathcal{L}^M\mathbf{v} = \mathbf{0}, \tag{38}$$

where $\mathcal{H}$ is the Bukhgeim–Hilbert transform in (20).

We consider (38) on $L = (-l, l)$, where for each $x \in (-l, l)$ and $n \geqslant M$, the nth component yields

$$\begin{aligned} v_{-n}(x) - \frac{\mathrm{i}}{\pi}\int_{-l}^{l}\frac{v_{-n}(s)}{x-s}\mathrm{d}s \\ = -\frac{\mathrm{i}}{\pi}\int_\Lambda \frac{v_{-n}(\zeta)}{\zeta - x}\mathrm{d}\zeta - \frac{\mathrm{i}}{\pi}\int_\Lambda \left\{\frac{\mathrm{d}\zeta}{\zeta - x} - \frac{\mathrm{d}\overline{\zeta}}{\overline{\zeta} - x}\right\}\sum_{j=1}^{\infty} v_{-n-2j}(\zeta)\left(\frac{\overline{\zeta} - x}{\zeta - x}\right)^j \\ - \frac{\mathrm{i}}{\pi}\int_{-l}^{l}\left\{\frac{\mathrm{d}\zeta}{\zeta - x} - \frac{\mathrm{d}\overline{\zeta}}{\overline{\zeta} - x}\right\}\sum_{j=1}^{\infty} v_{-n-2j}(\zeta)\left(\frac{\overline{\zeta} - x}{\zeta - x}\right)^j. \end{aligned} \tag{39}$$

Since the last integral in (39) ranges over the reals, it vanishes. The remaining two integrals in the right-hand side give $F_{-n}(x)$ in (35), and (39) becomes

$$[I - \mathrm{i}H_\mathrm{t}](v_{-n})(x) = F_{-n}(x), \quad x \in L, \quad n \geqslant M, \tag{40}$$

where H_t is the finite Hilbert transform in (28). For each $n \geqslant M$, by proposition 3.1, $v_{-n}|_L$ is determined as the unique solution in $L^2(-l, l)$ of (40).

Note that the equation (40) may not have any solution for an arbitrary right-hand side in $L^2(-l, l)$. However, in our inverse problem, the function F_{-n} already belongs to the range of

$I - \mathrm{i}H_{\mathrm{t}}$, so that the solution exists. Moreover, since the range is open, (40) is uniquely solvable in a sufficiently small L^2-neighborhood of F_{-n}.

With v_{-n} now known on $\Lambda \cup L$ for $n \geqslant M$, we apply the Bukhgeim–Cauchy integral formula (19) to find v_{-n} for $n \geqslant M$ in Ω^+.

Using again the convolution formula (24), now in Ω^+, we determine u_{-n} for $n \geqslant M$ inside Ω^+. In particular we recovered u_{-M-1}, u_{-M}.

Recall that $u_0, u_{-1}, u_{-2}, \ldots, u_{-M}, u_{-M-1}$ satisfy

$$\overline{\partial} u_{-M+j} = -\partial u_{-M+j-2} - \left[(a - k_{-M+j-1})u_{-M+j-1}\right], \quad 1 \leqslant j \leqslant M, \tag{41a}$$

$$u_{-M+j}|_{\Lambda} = g_{-M+j}. \tag{41b}$$

We solve (41) iteratively for $j = 1, 2, \ldots, M$, as a Cauchy problem for the $\overline{\partial}$-equation with partial boundary data on Λ,

$$\overline{\partial} w = \Psi, \quad \text{in } \Omega^+, \tag{42a}$$

$$w = \psi \quad \text{on } \Lambda, \tag{42b}$$

via the Cauchy–Pompeiu formula [33]:

$$w(z) = \frac{1}{2\pi \mathrm{i}} \int_{\partial\Omega^+} \frac{w(\zeta)}{\zeta - z} \mathrm{d}\zeta - \frac{1}{\pi} \iint_{\Omega^+} \frac{\Psi(\zeta)}{\zeta - z} \mathrm{d}\xi\, \mathrm{d}\eta, \quad \zeta = \xi + \mathrm{i}\eta, \quad z \in \Omega^+. \tag{43}$$

For $\Psi \in L^p(\Omega)$, $p > 2$, and $\psi \in L^p(\Lambda)$, any w defined by (43) solves (42a). However, for the boundary condition (42b) to be satisfied the following compatibility condition needs to hold: by taking the limit $\Omega^+ \ni z \to z_0 \in \partial\Omega^+$ in (43) and using the Sokhotski–Plemelj formula [23] in the first integral, and the continuous dependence on z of the area integral [33, theorem 1.19], the trace $w|_{\partial\Omega^+}$ and Ψ must satisfy

$$w(z_0) = \frac{1}{2\pi \mathrm{i}} \int_{\partial\Omega^+} \frac{w(\zeta)}{\zeta - z_0} \mathrm{d}\zeta + \frac{1}{2} w(z_0) - \frac{1}{\pi} \iint_{\Omega^+} \frac{\Psi(\xi, \eta)}{(\xi - z_0) + \mathrm{i}\eta} \mathrm{d}\xi\, \mathrm{d}\eta, \quad z_0 \in \partial\Omega^+.$$

In our inverse problem this compatibility condition is already satisfied for $z_0 \in \Lambda$. We use this compatibility condition for $z_0 \in L$, to recover the missing boundary data $w|_L$. More precisely, by proposition 3.1, $w|_L$ is the unique solution of

$$[I - \mathrm{i}H_{\mathrm{t}}]w(z_0) = \frac{1}{\pi \mathrm{i}} \int_{\Lambda} \frac{\psi(\zeta)}{\zeta - z_0} \mathrm{d}\zeta - \frac{2}{\pi} \iint_{\Omega^+} \frac{\Psi(\xi, \eta)}{(\xi - z_0) + \mathrm{i}\eta} \mathrm{d}\xi\, \mathrm{d}\eta, \quad z_0 \in L. \tag{44}$$

If $\psi \in L^p(\Lambda)$, $p \geqslant 2$, then (44) provides a unique solution $w|_L \in L^p(-l, l)$. Moreover, for $\Psi \in L^p(\Omega)$, $p > 2$, the solution w of (42a) is provided by (43) and lies in $W^{1,p}(\Omega)$. In the iteration, the right-hand side of (41a) is again in $L^p(\Omega)$, and the iteration can proceed.

We solve repeatedly (41) for $j = 1, \ldots, M$ to recover u_{-1} and u_0 in Ω^+. *A priori*, from the regularity of the solution of the forward problem, we known that $u_{-1}, u_0 \in C^{1,\mu}(\overline{\Omega})$ so that the source f is recovered pointwise by

$$f|_{\Omega^+}(z) = 2\,\mathrm{Re}\,(\partial u_{-1}(z)) + (a(z) - k_0(z))\, u_0(z), \quad z \in \Omega^+ \tag{45}$$

as a $C^{\mu}(\overline{\Omega^{+}})$-map. □

We summarize below in a stepwise fashion the reconstruction of f in the convex hull Ω^{+} of the boundary arc Λ. Recall that L is the segment joining the endpoints of Λ.

Reconstruction procedure: consider the data $\mathbf{u}|_{\Lambda}$.

(a) Using formula (24), and data $\mathcal{L}^{M}\mathbf{u}$ on Λ, determine the traces $\mathcal{L}^{M}\mathbf{v}|_{\Lambda}$ on Λ.

(b) Recover the traces $\mathcal{L}^{M}\mathbf{v}|_{L}$ pointwise on L as follows:

  (1) Using $\mathcal{L}^{M}\mathbf{v}|_{\Lambda}$, compute by formula (35), the function F_{-n}, for each $n \geqslant M$.

  (2) Recover for each $n \geqslant M$, the trace $v_{-n}|_{L}$ by solving (40).

(c) By Bukhgeim–Cauchy formula (19), extend v_{-n} for $n \geqslant M$ from the boundary $\Lambda \cup L$ to Ω^{+}.

(d) Using again formula (24), now in Ω^{+}, recover u_{-n} for $n \geqslant M$ inside Ω^{+}.

(e) Using u_{-M-1}, u_{-M}, recover the modes $u_{-M+1}, u_{-M+2}, \ldots, u_{-1}, u_{0}$ recursively as follows:

  (3) Using data $u_{-M+1}|_{\Lambda}$, recover the trace $u_{-M+1}|_{L}$ by solving (44).

  (4) Using $u_{-M+1}|_{\Lambda\cup L}$, recover u_{-M+1} inside Ω^{+} by the Cauchy–Pompeiu formula (43).

  (5) Now iterate the steps (e(3)) and (e(4)) to find the modes $u_{-M+2}, \ldots, u_{-2}, u_{-1}, u_{0}$ in Ω^{+}.

(f) Recover $f|_{\Omega^{+}}$ by formula (45).

5. Numerical results

To illustrate the numerical feasibility of the proposed method and its extensibility to general settings, in this section we present the results of three numerical experiments: the first one considers the noiseless data case, the second one considers a noise due to the modeling, and the third one consider a 5% random noise added to the data of the second experiment. The rigorous analysis on the numerical methods employed below requires further study and is left for a separate discussion.

The domain Ω is the unit disk, the measurement boundary Λ is the upper semicircle, and Ω^{+} is the upper semidisk. The numerical experiments consider the boundary value problem (29) with the attenuation

$$a(z) = \mu_{\mathrm{s}}(z) + \mu_{\mathrm{a}}(z),$$

where μ_{s}, and μ_{a} are the scattering and absorption coefficients, respectively.

In the first numerical experiment $a \in C^{2}(\overline{\Omega})$ and the scattering kernel is homogeneous with

$$k(\boldsymbol{\theta}\cdot\boldsymbol{\theta}') = \frac{\mu_{\mathrm{s}}}{2\pi}\left[1 + 2t(\boldsymbol{\theta}\cdot\boldsymbol{\theta}') + 2t^{2}\cos(2\arccos(\boldsymbol{\theta}\cdot\boldsymbol{\theta}'))\right], \tag{46}$$

where t is an anisotropy parameter.

In contrast, the second numerical experiment uses a *discontinuous* absorption coefficient μ_{a},

$$\mu_{\mathrm{a}}(z) = \begin{cases} 2, & \text{in } B_{1}; \\ 1, & \text{in } B_{2}; \\ 0.1, & \text{otherwise}, \end{cases} \tag{47}$$

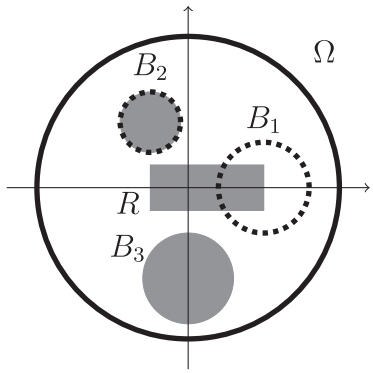

Figure 1. Domain Ω and inclusions; the dotted circles (B_1 and B_2) indicates highly absorbing regions, while gray regions (B_2, R and B_3) are support of internal sources.

and a homogeneous scattering kernel k of *infinite* Fourier content. More precisely, we work with the two dimensional Henyey–Greenstein (Poisson) kernel

$$k(\boldsymbol{\theta}\cdot\boldsymbol{\theta}') = \mu_{\mathrm{s}}\frac{1}{2\pi}\frac{1-t^2}{1-2t\boldsymbol{\theta}\cdot\boldsymbol{\theta}'+t^2}, \tag{48}$$

where t is an anisotropy parameter. Note that (46) comes from the quadratic truncation of (48).

Throughout this section, $\mu_{\mathrm{s}} \equiv 3$ and $t = 1/2$ are used, and computations are processed in the standard double precision arithmetic. The parameter $t = 1/2$ yields an anisotropic scattering half way between the ballistic ($t = 0$) regime and an isotropic scattering regime ($t = 1$). The value of the parameter μ_{s} yields that, on average, a particle scatters after running straight every $1/3$ of the unit path length. These parameter choices are meaningful in certain optical regimes, where the diffusion approximation would not hold.

Let $R = (-0.25, 0.5)\times(-0.15, 0.15)$ be a rectangular, and

$$\begin{aligned}
B_1 &= \{(x,y) : (x-0.5)^2 + y^2 < 0.3^2\},\\
B_2 &= \left\{(x,y) : (x+0.25)^2 + \left(y - \frac{\sqrt{3}}{4}\right) < 0.2^2\right\}, \quad \text{and}\\
B_3 &= \{(x,y) : x^2 + (y+0.6)^2 < 0.3^2\}
\end{aligned}$$

be circular regions inside Ω as illustrated in figure 1. The source term

$$f(z) = \begin{cases} 2, & \text{in } R;\\ 1, & \text{in } B_2\cup B_3;\\ 0, & \text{otherwise,}\end{cases}$$

used to generate the boundary data on Λ_+ is to be reconstructed in the upper semidisk Ω^+.

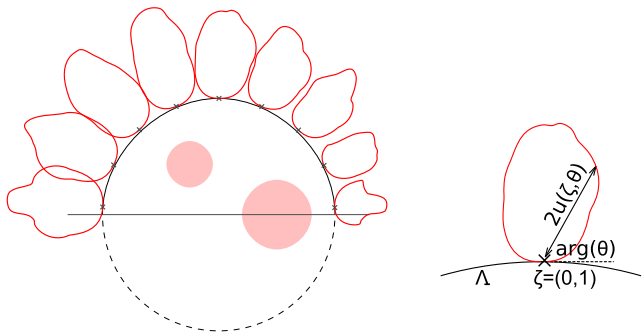

Figure 2. Boundary data $u|_{\Lambda_+}$: (left) the measurement arc Λ lies in the upper half plane. Each red closed curve stands for $\zeta + 2u(\zeta, \boldsymbol{\theta})$ for $\boldsymbol{\theta} \in \mathbf{S}^1$ at $\zeta \in \Lambda$ indicated by the cross symbol ($\times$); (right) magnification of $u(\zeta, \boldsymbol{\theta})$ at $\zeta = (0, 1)$.

In the first example the absorption coefficient is a C^2-smoothen version of the discontinuous case in (47). Namely, for $\epsilon = 0.05$,

$$\mu_{\mathrm{a}}(z) = \begin{cases} 2, & \text{in } \{z : \mathrm{dist}(z, \partial B_1) \geqslant \epsilon\} \cap B_1; \\ 1, & \text{in } \{z : \mathrm{dist}(z, \partial B_2) \geqslant \epsilon\} \cap B_2; \\ 0.1, & \text{in } \{z : \mathrm{dist}(z B_1) \geqslant \epsilon\} \cap \{z : \mathrm{dist}(z B_2) \geqslant \epsilon\}, \end{cases}$$

while in the ϵ-neighborhoods of ∂B_1 and ∂B_2 we use some translations and scalings of the quintic polynomial $-(|z| - 1)^3(6|z|^2 + 3|z| + 1)$, $|z| \leqslant 1$, to define $\mu_{\mathrm{a}} \in C^2(\overline{\Omega})$.

For our inverse problem, the 'measured' data (2) is generated by the numerical computation of the corresponding forward problem (1) in $\Omega \times \mathbf{S}^1$, where we retain the trace of the solution $u|_{\Lambda_+}$ and disregard the rest.

Note the contribution to the data of radiation coming from the source supported in the lower half of the rectangle R and from the ball B_3.

The numerical solution of the forward problem is obtained by the piecewise constant approximation method in [11], where the spatial domain Ω is divided into 4, 823, 822 triangles (the maximum diameter is approximately 0.0025), and 360 equi-directions are considered on $\mathbf{S}^1$. The boundary $\partial\Omega$ is approximated by 5, 234 equi-length segments, to yield 2, 617 spatial measurement nodes assigned on Λ.

The computed data in the first example is depicted in figure 2. In there, for $\zeta \in \Lambda$ (indicated by $\times$), the red closed curves represent $\zeta + 2u(\zeta, \boldsymbol{\theta})$, with computed $u(\zeta, \boldsymbol{\theta})$. The zero incoming flux boundary condition can be observed on the computed radiation, where the curves do not enter Ω.

In our numerical reconstruction, the domain of interest Ω^+ is partitioned into a triangular mesh without any prior information on R and B_i, $i = 1, 2, 3$. The number (8, 631) of triangles in this mesh is much less than that the number (4, 823, 822) of triangles used in the computation in the forward problem, thus avoiding an inverse crime. The attenuation coefficient a is assumed known in $\overline{\Omega}$. The triangular mesh induces 157 nodes on Λ and 100 nodes on L. Series (19), (24), and (35) are truncated with Fourier modes greater than or equal to -128.

The Hilbert transform in (27) is computed by a method proposed by the authors in [13]. All the integrations are approximated by the composite mid-point rule with equi-spaced intervals. The integrating factors in (25) are computed with 100 subintervals and 360 velocities, and the

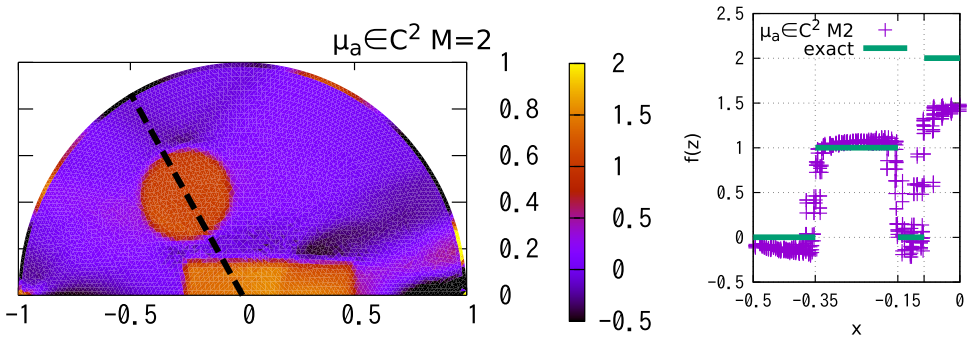

Figure 3. Numerically reconstructed $f(z)$ for polynomial type scattering kernel (46) and $\mu_a \in C^2(\Omega)$. (left) The profile of reconstructed f in the domain of interest Ω^+; (right) the section on the dotted line.

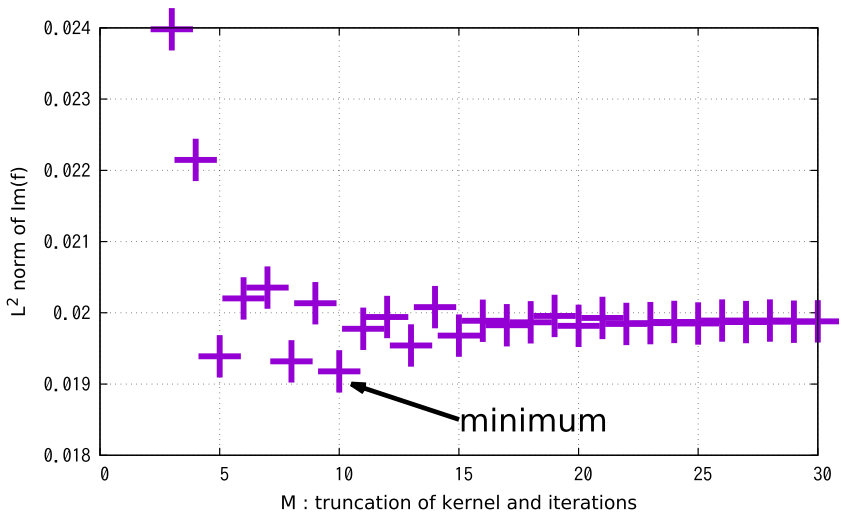

Figure 4. L^2 norm of the imaginary part of the reconstructed f for varying cutoff parameter M in the range $0 \leqslant M \leqslant 30$. The minimum is attained at $M = 10$. The values for $M = 0, 1, 2$ are greater than 0.024, and are not shown in the graph.

integral equations (40) and (44) are computed with 1, 666 subintervals (so that $\Delta x = 2/1666 \approx 0.0012$ on L is about the same with the length $\pi/2617$ of the partition on the arc Λ). Of particular interest, and key to our procedure, is the numerical computation of the integral equations (40) and (44), which is done via the collocation method with the numerical integration rule

$$[I - \mathrm{i}H_{\mathrm{t}}]u(x_i) \approx u(x_i) - \frac{\mathrm{i}}{\pi}\sum_{j\neq i}\frac{u(x_j)}{x_i - x_j}\Delta x.$$

Except for the implicit regularization due to the discretization, no other regularization method is explicitly employed in numerical implementation. The numerical reconstruction takes approximately 115 s by OpenMP parallel computation on two Xeon E5-2650 v4 (2.20 GHz, 12 cores) processors.

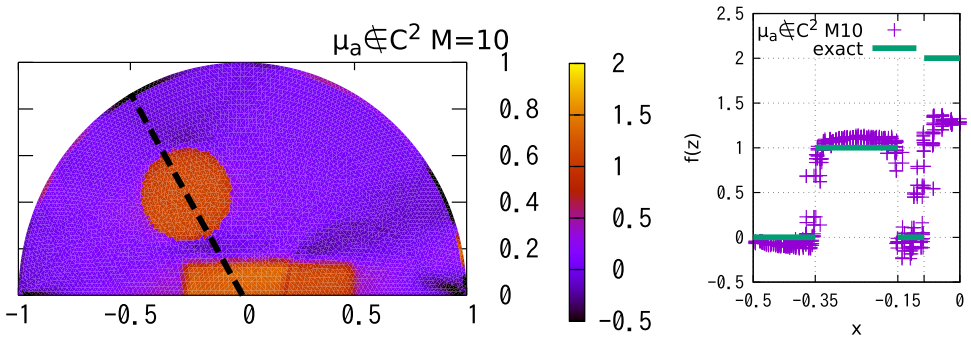

Figure 5. Numerically reconstructed $f(z)$ for the case with discontinuous μ_a (47) and Poisson kernel (48).

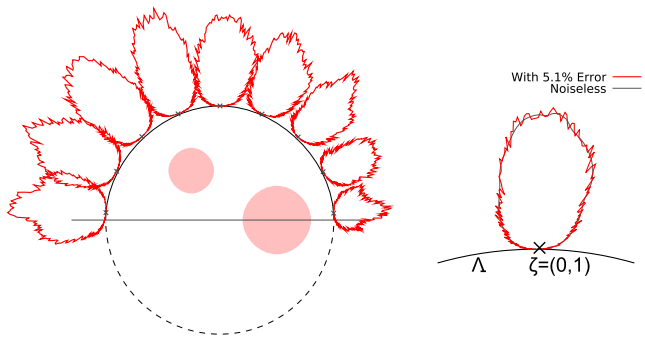

Figure 6. Boundary data $u|_{\Lambda_+}$ with relative 5.1% errors in L^2 sense; (left) the measurement arc Λ lies in the upper half plane; (right) comparison of $u(\zeta, \boldsymbol{\theta})$ at $\zeta = (0, 1)$ between 5.1% noisy data (red) and the original data (gray) in figure 2.

Figure 3 depicts numerical reconstruction results: on the left is the profile of reconstructed $f(z)$, and on the right is its section on the dotted line ($y = -\sqrt{3}x$). In the figure the support of $f(z)$ is successfully reproduced. The reconstructed source f away from the segment L is quantitatively in fine agreement with the exact one. However the accuracy of the reconstruction decreases at points on the support of f which are close to the line segment L. One of the reasons is the ill-posedness in equation (40), which we currently mitigate solely via the discretization. For a more accurate numerical reconstruction at such points, the choice of a better regularizer is needed.

While the reconstruction method assumes a scattering kernel of polynomial type (finite Fourier sum), in the second example the data is computed using the forward model with the Poisson scattering kernel in (48), which has infinite Fourier content. For an estimate on the noise introduced via the truncation parameter of the scattering kernel, we refer to [13, proposition 3.2].

The degree M of the polynomial scattering kernel should be chosen in advance. In here we use a criterion in [13], where the cut-off parameter M is chosen so that $\|\mathrm{Im}\, f\|_2$ is minimized. Figure 4 shows computed $\|\mathrm{Im}\, f\|_2$ obtained from the same measurement data, while varying M. For $0 \leqslant M \leqslant 30$, the minimum is achieved at $M = 10$. Figure 5 shows reconstructed results, where, according to our cutoff criterion, (41) is solved iteratively ten times.

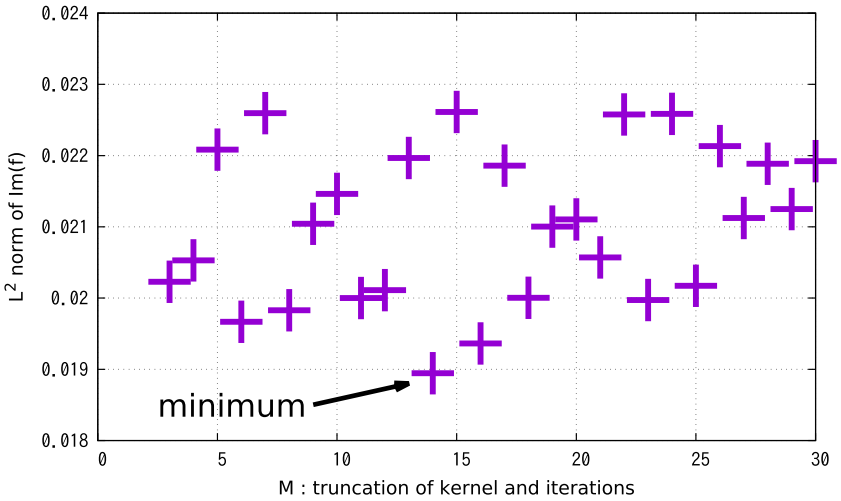

Figure 7. L^2 norm of the imaginary part of the reconstructed f from measurement data with added 5.1% relative error, and a varying cutoff parameter $0 \leqslant M \leqslant 30$. At $M = 14$ the minimum is achieved.

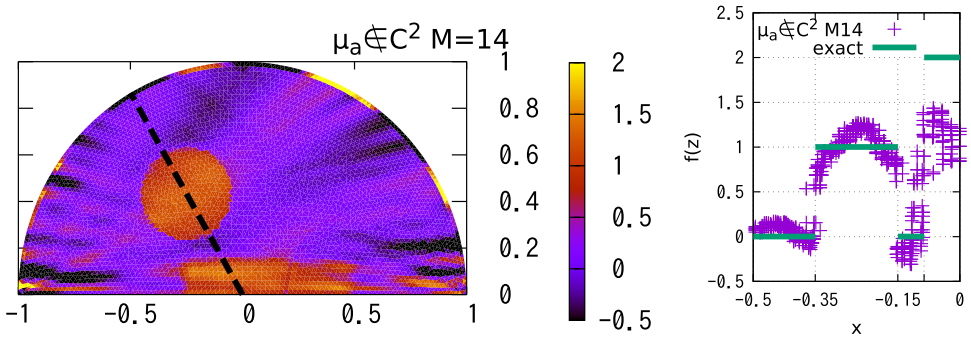

Figure 8. Numerically reconstructed $f(z)$ for measurement data 5.1% errors in figure 6 with discontinuous μ_a (47) and Poisson kernel (48).

Even though the smoothness and finiteness hypotheses in theorem 4.1 are violated, the numerical results are in agreement with the results in the first example (where all the hypotheses in theorem 4.1 were satisfied). This illustrates the robustness of the proposed reconstruction method with respect to the regularity of the coefficients, and indicates that the reconstruction result in theorem 4.1 may hold under more relaxed hypotheses.

To illustrate the robustness with respect to the noisy data, we exhibit the numerical reconstruction from data with added relative error in the L^2 sense of 5.1%. As in the second example, the forward model has the discontinuous μ_a in (47), and the scattering kernel in (48) of infinite Fourier content.

Figure 6 depicts noisy data generated with the built-in pseudo random routines in the programming language C++. The same *a posteriori* criterion, which minimizes $\|\mathrm{Im}\, f\|_2$ for $0 \leqslant M \leqslant 30$, yields the cutoff parameter $M = 14$; see figure 7. In particular, in the noisy case, we solve 14-many boundary value problems (41). Note that the cutoff parameter M is different in the noiseless case than in the noisy case. The numerically reconstructed source in

figure 8, which uses measurements with 5.1% noise, still shows a reasonably good agreement with the exact source. A better understanding of the influence of the scattering and absorption coefficients to the instability, and an appropriate regularization method is subject to further work.

Acknowledgments

The work of H Fujiwara was supported by JSPS KAKENHI Grant Numbers JP19H00641 and JP20H01821. The work of K Sadiq was supported by the Austrian Science Fund (FWF), Project P31053-N32. The work of A Tamasan was supported in part by the NSF Grant DMS-1907097.

Data availability statement

The data that support the findings of this study are available upon reasonable request from the authors.

ORCID iDs

Kamran Sadiq https://orcid.org/0000-0002-2197-2875
Alexandru Tamasan https://orcid.org/0000-0001-5456-6630

References

[1] Anikonov D S, Kovtanyuk A E and Prokhorov I V 2002 *Transport Equation and Tomography* (*Inverse and Ill-Posed Problems Series* vol 30) (Netherlands: Brill Academics)
[2] Bal G and Tamasan A 2007 Inverse source problems in transport equations *SIAM J. Math. Anal.* **39** 57–76
[3] Bukhgeim A L 1995 *Inversion Formulas in Inverse Problems* (*Linear Operators and Ill-Posed Problems*) ed M M Lavrentiev and L Y Savalev (New York: Plenum)
[4] Chandrasekhar S 1960 *Radiative Transfer* (New York: Dover)
[5] Choulli M and Stefanov P 1996 Inverse scattering and inverse boundary value problems for the linear Boltzmann equation *Commun. PDE* **21** 763–85
[6] Choulli M and Stefanov P 1999 An inverse boundary value problem for the stationary transport equation *Osaka J. Math.* **36** 87–104
[7] Dautray R and Lions J-L 1990 *Mathematical Analysis and Numerical Methods for Science and Technology* vol 4 (Berlin: Springer)
[8] Dunford N and Schwartz J 1957 *Linear Operators, Part I: General Theory* (New York: Wiley)
[9] Egger H and Schlottbom M 2014 An L^p theory for stationary radiative transfer *Appl. Anal.* **93** 1283–96
[10] Finch D V 2003 The attenuated x-ray transform: recent developments *Inside Out: Inverse Problems and Applications* (*Mathematical Sciences Research Institute Publication* vol 47) (Cambridge: Cambridge University Press) pp 47–66
[11] Fujiwara H 2020 Piecewise constant upwind approximations to the stationary radiative transport equation *Mathematical Analysis of Continuum Mechanics and Industrial Applications III, CoMFoS* (*Mathematics for Industry* vol 34) (Berlin: Springer) pp 35–45
[12] Fujiwara H, Sadiq K and Tamasan A 2019 A Fourier approach to the inverse source problem in an absorbing and anisotropic scattering medium *Inverse Problems* **36** 015005
[13] Fujiwara H, Sadiq K and Tamasan A 2020 Numerical reconstruction of radiative sources in an absorbing and nondiffusing scattering medium in two dimensions *SIAM J. Imaging Sci.* **13** 535–55

[14] Fujiwara H, Sadiq K and Tamasan A 2021 Partial inversion of the 2D attenuated x-ray transform with data on an arc *Inverse Probl. Imaging* https://doi.org/10.3934/ipi.2021047
[15] Han W, Eichholz J A, Huang J and Lu J 2011 RTE-based bioluminescence tomography: a theoretical study *Inverse Probl. Sci. Eng.* **19** 435–59
[16] Hubenthal M 2011 An inverse source problem in radiative transfer with partial data *Inverse Problems* **27** 125009
[17] Klose A D, Ntziachristos V and Hielscher A H 2005 The inverse source problem based on the radiative transfer equation in optical molecular imaging *J. Comput. Phys.* **202** 323–45
[18] Koppelman W and Pincus J D 1959 Spectral representations for finite Hilbert transformations *Math. Z.* **71** 399–407
[19] Larsen E W 1975 The inverse source problem in radiative transfer *J. Quant. Spectrosc. Radiat. Transfer* **15** 1–5
[20] Mikhlin S G and Prössdorf S 1986 *Singular Integral Operators* (Berlin: Springer)
[21] Mokhtar-Kharroubi M 1997 *Mathematical Topics in Neutron Transport Theory* (Singapore: World Scientific)
[22] Monard F and Bal G 2019 Inverse source problems in transport via attenuated tensor tomography (arXiv:1908.06508v1)
[23] Muskhelishvili N I 2008 *Singular Integral Equations* (New York: Dover)
[24] Natterer F 1986 *The Mathematics of Computerized Tomography* (New York: Wiley)
[25] Okada S and Elliott D 1991 The finite Hilbert transform in $\mathcal{L}^2$ *Math. Nachr.* **153** 43–56
[26] Sadiq K and Tamasan A 2015 On the range of the attenuated Radon transform in strictly convex sets *Trans. Am. Math. Soc.* **367** 5375–98
[27] Sadiq K and Tamasan A 2015 On the range characterization of the two-dimensional attenuated Doppler transform *SIAM J. Math. Anal.* **47** 2001–21
[28] Sadiq K, Scherzer O and Tamasan A 2016 On the x-ray transform of planar symmetric two-tensors *J. Math. Anal. Appl.* **442** 31–49
[29] Sharafutdinov V A 1997 Inverse problem of determining a source in the stationary transport equation on a Riemannian manifold *Mat. Vopr. Teor. Rasprostr. Voln.* **26** 236–42
Sharafutdinov V A 1999 *J. Math. Sci.* **96** 3430–3
[30] Smirnov A V, Klibanov M V and Nguyen L H 2019 On an inverse source problem for the full radiative transfer equation with incomplete data *SIAM J. Sci. Comput.* **41** 929B–52
[31] Stefanov P and Uhlmann G 2008 An inverse source problem in optical molecular imaging *Anal. PDE* **1** 115–26
[32] Tricomi F G 1957 *Integral Equations* (New York: Interscience)
[33] Vekua I N 1962 *Generalized Analytic Functions* (Oxford: Pergamon)
[34] Widom H 1960 Singular integral equations in L_p *Trans. Am. Math. Soc.* **97** 131
[35] Yi H C, Sanchez R and McCormick N J 1992 Bioluminescence estimation from ocean *in situ* irradiances *Appl. Opt.* **31** 822–30